Journal of *Marine Science and Engineering*

MDPI

Article

Research on Low-Frequency Vibration Monitoring Sensor Based on a Cantilever-Beam-Structured Triboelectric Nanogenerator

Xiu Xiao *, Qunyi Wang, Bohan Yao, Linan Guo, Chuanqing Zhu, Cong Zhao, Ling Liu and Minyi Xu

Dalian Key Laboratory of Marine Micro/Nano Energy and Self-Powered Systems, Marine Engineering College, Dalian Maritime University, Dalian 116026, China; xuminyi@dlmu.edu.cn (M.X.)
* Correspondence: xiaoxiu@dlmu.edu.cn

Abstract: Vibration sensing is of great significance in offshore engineering monitoring and safety detection. This paper presented a low-frequency vibration sensor (LV-TENG) based on a cantilever-beam-structured triboelectric nanogenerator, which can perform high-precision vibration sensing while conducting vibration energy collection effectively. The LV-TENG was composed of two aluminum electrode layers, a spring steel sheet covered with polytetrafluoroethylene (PTFE) and a first-order vibration mode structured frame. Under the excitation of external vibration, the spring steel sheet undergoes first-order modal vibrations between the aluminum electrodes and generates a periodically fluctuating electrical signal in the external circuit. The vibration profile of the cantilever beam was first analyzed theoretically to provide guidance for structural design. On this basis, the influence of the main structural parameters, including the structure of the Al electrode, the thickness of the steel plate, and the electronegative materials, on the output performance of LV-TENG was experimentally investigated and the structure was optimized to enhance electrical output. The results showed that the LV-TENG can accurately sense structure vibration with a frequency of 0.1 Hz to 5.0 Hz and an amplitude of 2.0 mm to 10.0 mm. The measured output voltage followed a positive linear relationship with frequency and the fitted correlation coefficient reached 0.994. The demonstration experiment indicated that the LV-TENG is expected to provide a new avenue for low-frequency vibration monitoring and can be used for structural health monitoring analysis in marine engineering.

Keywords: triboelectric nanogenerator; cantilever beam; low frequency vibration sensing; offshore platform

Citation: Xiao, X.; Wang, Q.; Yao, B.; Guo, L.; Zhu, C.; Zhao, C.; Liu, L.; Xu, M. Research on Low-Frequency Vibration Monitoring Sensor Based on a Cantilever-Beam-Structured Triboelectric Nanogenerator. *J. Mar. Sci. Eng.* **2023**, *11*, 838. https://doi.org/10.3390/jmse11040838

Academic Editor: Eugen Rusu

Received: 15 March 2023
Revised: 6 April 2023
Accepted: 12 April 2023
Published: 15 April 2023

1. Introduction

Vibration is a prevalent physical phenomenon in marine engineering, such as offshore platforms [1], ship piping systems [2], large ship machinery [3], and bridge structures [4]. In particular, there is a large quantity of mechanical equipment and piping systems on offshore platforms [5], whose vibration may induce local low-frequency resonance on the platform, and even cause fatigue damage to the platform structure. Vibration is generally considered to be negative and unavoidable. However, it is important to note that vibration is the basis for information transmission. Vibration itself contains a great deal of information about the operational safety of machinery and the health of structures, and the analysis and processing of relevant vibration information can help to identify safety hazards in time and avoid uncertain disasters [6–8]. Therefore, in order to ensure the safety of offshore structures, it is vital to carry out low-frequency vibration information collection and analysis.

With the development of the Internet, the Internet of Things (IoT) technology is gradually being widely used in the industrial sector. The rapid development of IoT relies on smart sensor technology, and the self-sustained technology based on energy capture is one of the main development directions for sensors [9–11]. In the field of vibration monitoring, self-powered vibration sensing through vibration energy harvesting has gradually

become a research hotspot. In 2012, ZhongLin Wang [12–16] proposed triboelectric nanogenerator (TENG) technology, which provides a fresh new idea for self-powered sensing. The triboelectric nanogenerator is a new microenergy harvesting technology based on the combination of charged effect and electrostatic induction effect between triboelectric materials [17–19]. It has the advantages of high efficiency, low cost, easy fabrication, small and compact structure, and is considered to have broad development and application prospects [20–22].

As mentioned above, vibration monitoring is an important part of the structural health monitoring (SHM) of marine engineering. The three main types of classical vibration monitoring sensors are mechanical, optical, and electrical. However, the high cost of power supply, short lifetime, and marine environmental pollution are still serious challenges at present [23,24]. As a new energy conversion technology, TENG has a natural advantage for obtaining mechanical energy and provides a viable solution for power supply and vibration monitoring. Currently, some TENG-related technologies have been proposed for vibration energy harvesting and vibration sensing [23,24]. Wang et al. [25] designed a triboelectric nanogenerator (CF-TENG) based on a harmonic resonator for self-powered vibration sensing. The sensor consisted of Polylactic acid(PLA), spring, aluminum, and copper electrodes. The CF-TENG had a resonant frequency of 15 Hz and could monitor a displacement amplitude of 15 mm at the vibration frequency of 21 Hz. Salauddin.MD et al. [26] proposed an EMG–TENG hybrid resonant nanogenerator (LFR-HN). The best output of this sensor occurred at a vibration frequency of 31.8 Hz. Seol et al. [27] designed an all-printed triboelectric nanogenerator vibration sensor. The optimum vibration frequency measurement range was 30–60 Hz. These vibration-sensing technologies are characterized by the spring-assistant structures and are often referred to as resonant vibration sensors. This type of sensor usually has a relatively high power density near the resonance frequency, but the working bandwidth is generally small. Beyond the resonance frequency range, the output of the sensor drops significantly and the accurate sensing of vibration becomes impossible. Therefore, Du et al. [28] fabricated a bouncing-ball-type TENG vibration sensor (BB-TENG). The sensor successfully achieved vibration energy harvesting from 10 Hz to 50 Hz using friction and electron transfer phenomena between PTFE balls and Cu membranes. Zhang et al. [29] designed a spherical three-dimensional triboelectric nanogenerator vibration sensor. It was composed of a Polyfluoroalkoxy sphere, aluminum electrodes, and a transparent housing. The sensor has a trigger frequency of 10 Hz and a maximum output of 57 V. Wang et al. [30] invented a TENG vibration sensor, which consisted of PU balls, PTFE, and copper. The sensor has a measuring range of 20–50 Hz, and can simultaneously monitor forward, reverse, left, right, and braking actions. Xiao et al. [31] proposed a honeycomb-structured triboelectric nanogenerator (HSI-TENG) for vibration energy harvesting and vibration monitoring. The HSI-TENG consisted of a copper membrane, a sponge base, PLA and PTFE balls, and was mainly used for vibration information monitoring from 10 Hz to 60 Hz. This type of sensor does not have the spring structure and is considered to be a nonresonant vibration sensor. The SHM in marine engineering generally requires the vibration sensors to work under low-frequency vibration conditions. The nonresonant vibration sensors have relatively a large operating bandwidth, but the trigger frequency is usually high, which does not meet the requirements of SHM.

From the above literature review, it can be seen that the TENG-based vibration sensing technology has provided a new way for self-powered vibration detection. However, due to the extremely low energy density, the research on low-frequency vibration sensing has encountered great difficulties and the published achievement is quite rare. Since vibration with frequency lower than 5 Hz is common on marine structures such as offshore platforms, it is urgent to study a robust high-precision vibration monitoring and sensing technology under low-frequency vibrations. In this paper, a low-frequency vibration sensor named LV-TENG was proposed based on a cantilever-beam-structured triboelectric nanogenerator. The sensor structure was optimized by structure parameter sensitivity

analysis and experiments to enhance output performance. It was designed to conduct vibration sensing from 0.1 Hz to 5.0 Hz with high precision while realizing vibration energy capture. The LV-TENG has presented a fresh new approach to low-frequency vibration monitoring and has broad application prospects in the SHM of marine engineering.

2. Materials and Methods

The application scenario and working principle of the LV-TENG are shown in Figure 1. As depicted in Figure 1a, the LV-TENG can be used to monitor vibration information in a variety of scenarios, including offshore platforms, cross-sea bridges, etc. The LV-TENG uses PolyLactic Acid (PLA) as the basic frame, and a stainless-steel sheet is fixed in the middle to form the cantilever beam structure (Figure 1b). The length and width of the cantilever beam are set to 100 mm and 50 mm, respectively. The surfaces of the spring steel sheet are covered with Polytetrafluoro-Ethylene (PTFE) membranes to act as the dielectric layers. Once excited by external vibration, the spring steel sheet undergoes first-order vibration. The inner side of the PLA frame is designed according to the vibration mode profile of the cantilever beam so as to ensure full utilization of the deformation of the cantilever beam and increase the effective contact area. Aluminum (Al) films are attached to the upper and lower sides of the frame as the electrode layers. Surface micro/nano structure is one of the major methods to enhance the output performance of triboelectric nanogenerator. As indicated by M. Salauddin [32], the specific surface areas within the effective range of charge transfer can be very large when the nanostructures are in the compressive state, thus increasing the total amount of charge transfer. Therefore, the PTFE film was sanded with a 10,000-mesh sandpaper to improve the electrical output of the LV-TENG. Figure 1c exhibits the images of the original and sanded PTFE surfaces. It can be seen that the surface treatment results in a much rougher surface that can produce a larger contact area when in contact with the Al electrode.

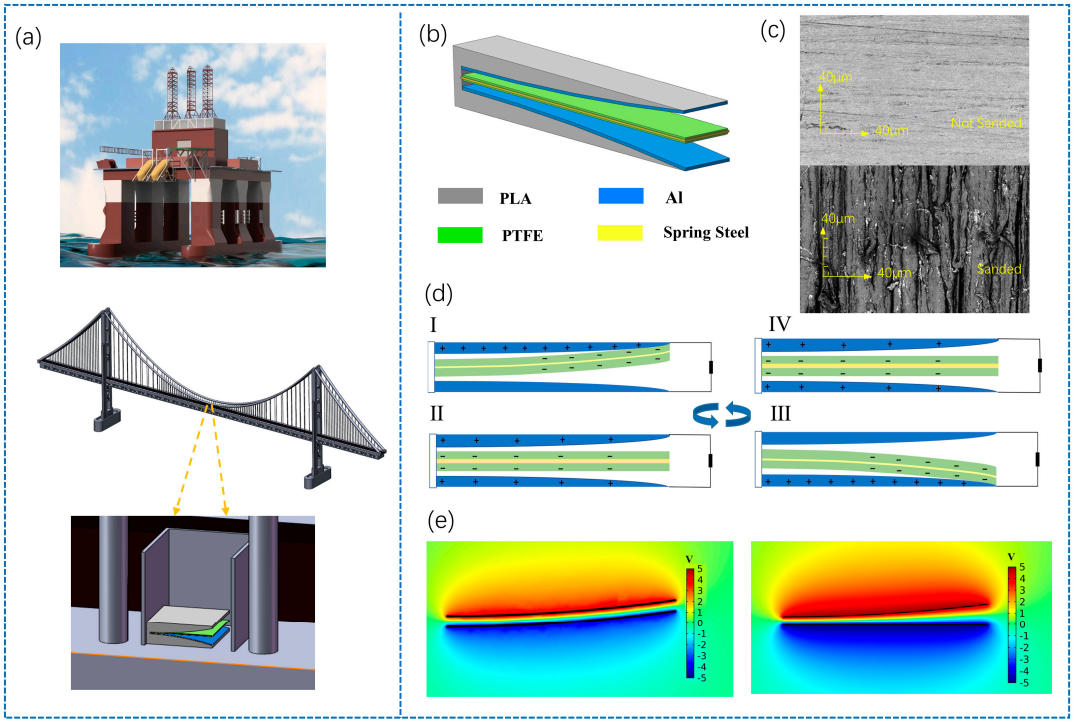

Figure 1. Application scenarios and working principle of LV-TENG. (**a**)Application scenarios of the LV-TENG; (**b**) Schematic diagram of the LV-TENG; (**c**) SEM images of the original and sanded PTFE surfaces; (**d**) Operating principle of the LV-TENG; (**e**) Simulations of the electric potential distributions of the LV-TENG.

The working principle of the LV-TENG is demonstrated in Figure 1d. When subjected to an external excitation, the spring steel sheet with PTFE attached starts to vibrate with the equations of the Galileo–Kirchoff–Lagrange bended beam. A mechanical model approach is proposed in Part 3 to design the specific structure of the Al electrodes and make the vibration process robust. As the spring steel sheet comes into contact with the upper Al electrode, the contact surfaces between the PTFE and Al electrodes generate equal amounts of opposite charges due to the different electronegativity of the materials (Figure 1d(I)). As the spring steel vibrates downward, an electrical potential is established and the electrons are driven from the bottom Al electrode to the top Al electrode through the external circuit. Once the vibrating beam returns to its initial position, the positive charges on the top Al electrode are neutralized and an electrostatic balance is reached temporarily (Figure 1d(II)). When the beam continues to go downward, the inductive electrons flow in the reverse direction until the PTFE attached on the steel sheet reaches out to the bottom Al electrode and the potential difference between the two Al electrodes reaches its maximum again (Figure 1d(III)). As the steel sheet moves upward, an opposing electric field is induced (Figure 1d(IV)). Thus, a complete sinusoidal electrical output is formed and the vibration of the steel sheet is converted into electrical information. In addition, a finite element analysis was carried out using COMSOL software (COMSOL Co., Ltd., Beijing, China) to illustrate the operation of the LV-TENG. Figure 1e shows the simulated potential distribution of the PTFE membrane and the Al electrode at different locations. It can be seen that the electric potential increases as the separation distance between the PTFE film and the Al electrode decreases, which is consistent with the previous analysis.

3. Results and Discussions

3.1. Structural Optimization of LV-TENG

A test system was built to measure the output performance of the LV-TENG. As shown in Figure 2a, the LV-TENG was mounted on an electrodynamic shaker ((JZK-20, SINOCERA, Suzhou, China) that was used as an external excitation source. The shaker was driven by an external amplifier (YE5872A, SINOCERA, Suzhou, China), which accepted vibration signals from the function generator (YE1311, SINOCERA, Suzhou, China), and can generate various forms of vibration with different frequencies and amplitudes. The vibration energy and information were then converted into electrical signals through the LV-TENG. A Keithley 6514 electrometer is used to measure the output performance of the LV-TENG.

The LV-TENG works based on the principle of electrostatic induction and triboelectrification, so the selection of electronegative material is crucial to the output performance of the device. Three electronegative materials, i.e., FEP, PTFE, and Ecoflex, were tested under a vibration frequency of 0.5 Hz and a vibration amplitude of 6.0 mm, and the results are displayed in Figure 2b. It can be seen that the use of the PTFE electrode exhibits superior output performance compared to the other two materials. More specifically, when the PTFE was adopted as the electrode material, the output voltage of the LV-TENG was 64% and 497% higher than that of the FEP and Ecoflex electrodes, respectively. This is because the PTFE has a stronger electronegativity and a higher ability to attract electrons than the FEP and Ecoflex according to the Triboelectric Nanoelectricity Materials Gain and Loss of Electrons table [33], which effectively improves the electrical output performance of the TENG. Therefore, the PTFE is used as the flexible electrode.

The vibrations with low frequency and low amplitude are difficult to measure due to the small energy density. Therefore, it is critical to obtain the first-order vibration profile of the cantilever beam so as to make sure that the structures of the Al electrodes and the dielectric material are effectively matched. A mechanical analysis was carried out to design the specific structure of the LV-TENG. As shown in Figure 2c(i), the stainless-steel sheet was simplified to an equal-section cantilever beam. Assuming that any point x on the beam vibrates periodically in the y direction, the vibration profile at this point is shaped as:

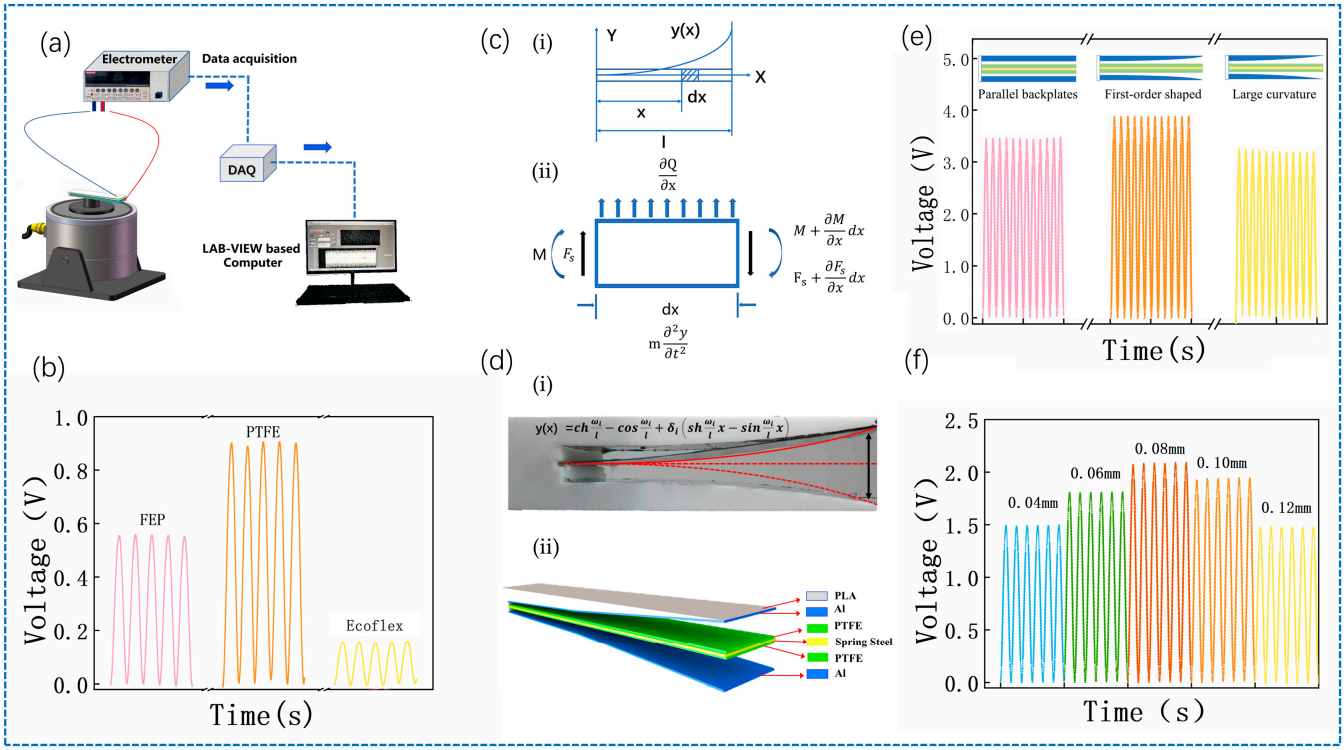

Figure 2. Structure optimization of the LV-TENG. (**a**) Test system; (**b**) Effect of electronegative materials on the electrical output of the LV-TENG; (**c**) Model simplification and force analysis of cantilever beam; (**d**) Dynamic vibration profile of the cantilever beam and the schematic diagram of the Al electrodes; (**e**) Effect of electrode structure on the output of the LV-TENG; (**f**) Effect of cantilever beam thickness on the output of the LV-TENG.

$$y(x,t) = Y(x)cos\omega t \tag{1}$$

where $y(x,t)$ is the displacement curve function of the cantilever beam, $Y(x)$ is the displacement of the cantilever beam at x, ω is the vibration frequency, and t represents time. The motion of the cantilever beam is determined by the external load. Figure 2c(ii) shows the force analysis of the beam microelement. Assuming that the mass of the microelement is m, the inertial force acting on the element is $-m\left(\partial^2 y/\partial t^2\right)dx$. The elastic recovery force has the expression as in [34]:

$$\frac{\partial Q}{\partial x}dx = qd = \frac{\partial^2}{\partial x^2}\left(EI\frac{\partial^2 y}{\partial x^2}\right)dx \tag{2}$$

where $\frac{\partial Q}{\partial x}dx$ is the elastic restoring force acting on dx, and q is the distributed load. Since any microelement dx of the cantilever beam is subject to periodic vibration, i.e., the elastic recovery force and the inertial force are balanced, the motion equation of the cantilever beam can be expressed as [34]:

$$EI\frac{\partial^4 y}{\partial x^4} = -m\frac{\partial^2 y}{\partial t^2} \tag{3}$$

Combining the above motion equation with the Euler–Bernoulli equation, the D'Alembert principle, and the equations for the bending moment and shear force, the vibration profile is obtained as [34]:

$$y(x) = ch\frac{\omega_i}{l} - cos\frac{\omega_i}{l} + \delta_i\left(sh\frac{\omega_i}{l}x - sin\frac{\omega_i}{l}x\right) \tag{4}$$

In which,

$$\delta_i = -\frac{ch\varphi_i + cos\varphi_i}{sh\varphi_i + sin\varphi_i} \tag{5}$$

$$\omega_i = {\beta_i}^2 \sqrt{\frac{EI}{m}} \tag{6}$$

where ω_i is the cantilever beam inherent frequency, l is the length of the cantilever beam, β_i is the correlation coefficient, E is the modulus of elasticity, and I is the moment of inertia of the section.

In fact, the vibration profile of the cantilever beam was determined by its width, length, and thickness. The aspect ratio of the spring steel sheet was fixed for simplification, in which the length and width of the beam were set to 100 mm and 50 mm, respectively. Figure 2d shows the dynamic vibration pattern of the cantilever beam obtained by the above equations and a schematic diagram of the Al electrode structure thus designed. To confirm the above analysis, two electrode structures with different curve profiles were also designed, which were the parallel plate type and the large curvature type. The specific structures of the three Al electrodes are exhibited in Figure S1 of the supplementary. The output performances of the LV-TENG with different structured Al electrodes are shown in Figure 2e. Since the contact area between the Al electrode and the PTFE are maximized when they are well matched, the adoption of the Al electrode with the first-order vibration curve structure can effectively enhance the electrical output of the LV-TENG. This is coherent with the above analysis.

Moreover, as it can be seen from the expressions of the vibration profile and the natural frequency of the spring steel, the thickness of the cantilever beam is closely related to its vibration mode. Figure 2f shows the effect of spring steel thickness on the electrical output of the LV-TENG, in which the thickness of the cantilever beam is set to 0.04 mm, 0.06 mm, 0.08 mm, 0.10 mm, and 0.12 mm, respectively, and the external excitation has a frequency of 3.0 Hz and an amplitude of 4.0 mm. As the thickness of the spring steel increases, the output voltage of the LV-TENG shows a trend of first increasing and then decreasing. The electrical output reaches its maximum of 2.10 V at the thickness of 0.08 mm. The reason for this phenomenon is that, in the thickness range from 0.04 mm to 0.08 mm, the intrinsic frequency of the cantilever beam oscillator gradually increases to the external excitation frequency. The deformation of the spring steel and the contact area between the PTFE and Al electrodes is enlarged, resulting in the raise in electrical output. With the further increase of the cantilever beam thickness, the stiffness of the vibrator increases significantly and the bending deformation of the spring steel decreases. As a result, the output voltage of the LV-TENG starts to drop. Therefore, there is an optimal spring steel thickness of 0.08 mm for the current LV-TENG to achieve the best electrical output.

3.2. Output Performance of LV-TENG

For the vibration beam with a fixed structure, the vibration characteristics are mainly determined by external excitation. The LV-TENG was designed to capture vibration energy and vibration information under low-frequency vibrations. Therefore, a comprehensive sensitivity analysis of the vibration parameters on the output performance of the LV-TENG was performed under vibration frequencies from 0.1 Hz to 5.0 Hz in this part. The specific structural parameters suggested in the structural optimization were adopted in order to obtain the best electrical output.

Figure 3a,b display the output open-circuit voltage and short-circuit current of the LV-TENG under vibration frequencies from 0.1 Hz to 5.0 Hz. The vibration amplitude is fixed at 6.0 mm. Stable electrical output is obtained under the vibration conditions of concern and the pulse frequency of the electrical signal is positively correlated with the vibration frequency, indicating that the LV-TENG is capable of conducting low-frequency vibration monitoring. As the vibration frequency increased from 0.1 Hz to 5.0 Hz, the output voltage and current increased from 14.77 pA to 93.11 pA and from 0.47 V to

2.37 V, respectively. To better elucidate the responsiveness of the LV-TENG to low-frequency vibrations, the device was particularly tested under vibration frequency from 0.1 Hz to 0.9 Hz at 0.1 Hz intervals. The output peak voltage and current are shown in Figure 3c,d, where the vibration amplitude varied from 2.0 mm to 10.0 mm. It can be seen that with the increase in vibration parameters, the peak voltage and peak current increase continuously. Specifically, the peak voltage and current are 0.33 V and 8.48 pA at a vibration frequency of 0.1 Hz and a vibration amplitude of 2.0 Hz. As the vibration parameters increase to 0.9 Hz and 10.0 mm, the output peaks hike to 1.73 V and 57.41 pA. On the one hand, with the increase in vibration frequency, the contact–separation between the PTFE membrane and the Al electrode per unit of time increases, resulting in an increase in the total amount of transferred electrons, and the potential difference between the upper and lower aluminum electrodes enlarges. On the other hand, the increase in vibration amplitude amplifies the contact pressure and expands the contact area between the PTFE membrane and the Al electrode, which also causes the increase in transferred electrons and short-circuit current. Similar changes can be observed as the vibration frequency raised from 1.0 Hz to 5.0 Hz. The overall output performance of the LV-TENG is demonstrated in Figure 3e,f. The results indicate that the cantilever beam and the LV-TENG work robustly under the first-order vibration mode, which is coherent with the previous design and specification. Under the maximum vibration condition of f = 5.0 Hz and A = 10.0 mm, the peak open-circuit voltage and short-circuit current reach 8.35 V and 189.72 pA, respectively. Furthermore, the output power of the LV-TENG under the vibration frequency of 5 Hz and vibration amplitude of 10 mm was calculated, and the corresponding profile was exhibited in Figure S4 of the supplementary. With the increase in external load resistance, the output power first increases and then decreases, and the peak output power of 18.48 μW is obtained at the external resistance of 5.75 MΩ.

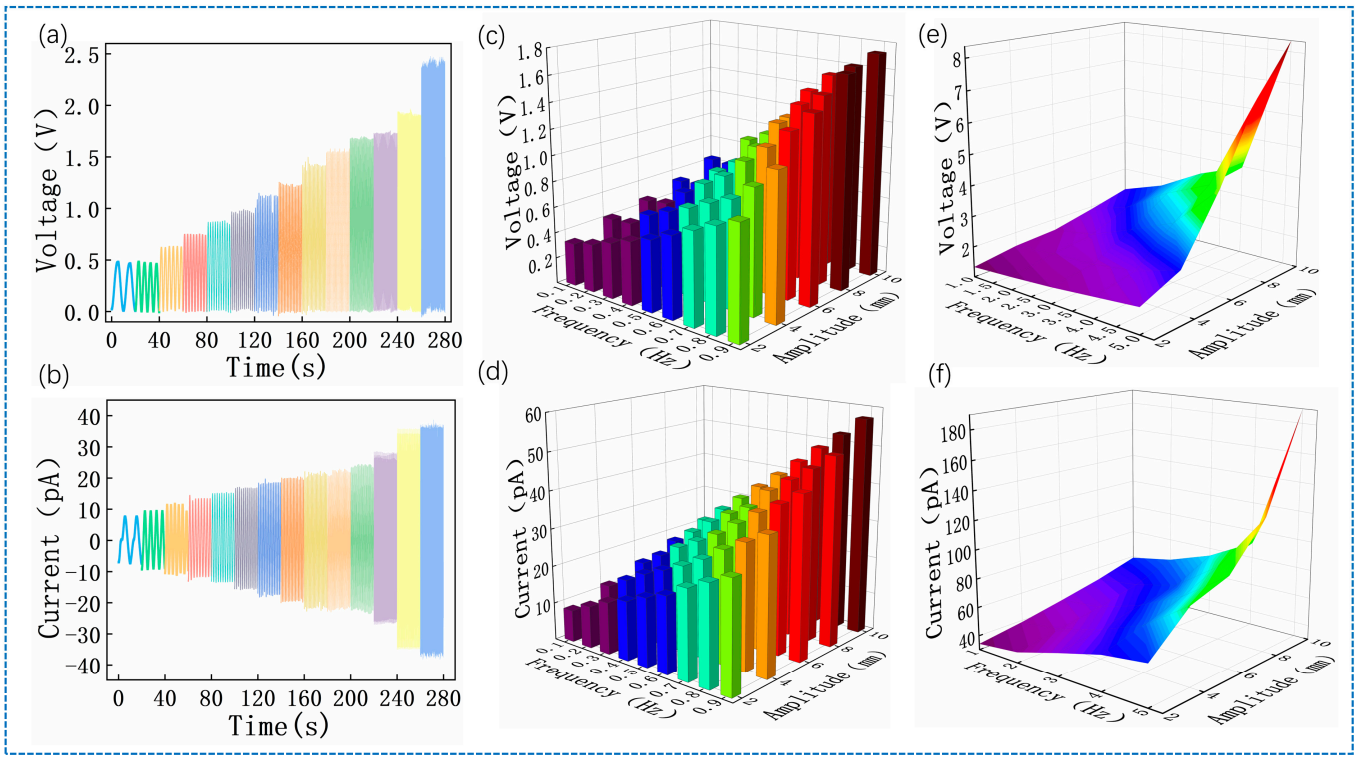

Figure 3. Output performance of the LV-TENG. (**a**) Open-circuit voltage and (**b**) short-circuit current at vibration amplitude of 6.0 mm and vibration frequencies from 0.1 Hz to 5.0 Hz; (**c**) Open-circuit voltage and (**d**) short-circuit current at vibration frequencies from 0.1 Hz to 0.9 Hz and vibration amplitudes from 2.0 mm to 10.0 mm; (**e**) Overall output open-circuit voltage and (**f**) short-circuit current of the LV-TENG.

3.3. Low-Frequency Vibration Sensing

According to the operation principle, the LV-TENG can be used as a low-frequency vibration sensor while conducting vibration energy collection. Figure 4a shows the output voltage of the LV-TENG under the external excitation of f = 2.0 Hz and A = 6.0 mm. A fast Fourier Transform (FFT) was performed on the output signal to convert it into vibration frequency information, and the result is presented in Figure 4b. It can be seen that the output vibration signal can reveal the frequency of the detected vibration with an error less than 1%. To confirm the ability of vibration frequency sensing in the LV-TENG, all the measured vibration signals under various vibration conditions were subjected to Fast Fourier Transform as shown in Figure 4c, which indicated that the vibration frequency error detected by the LV-TENG did not exceed 2%.

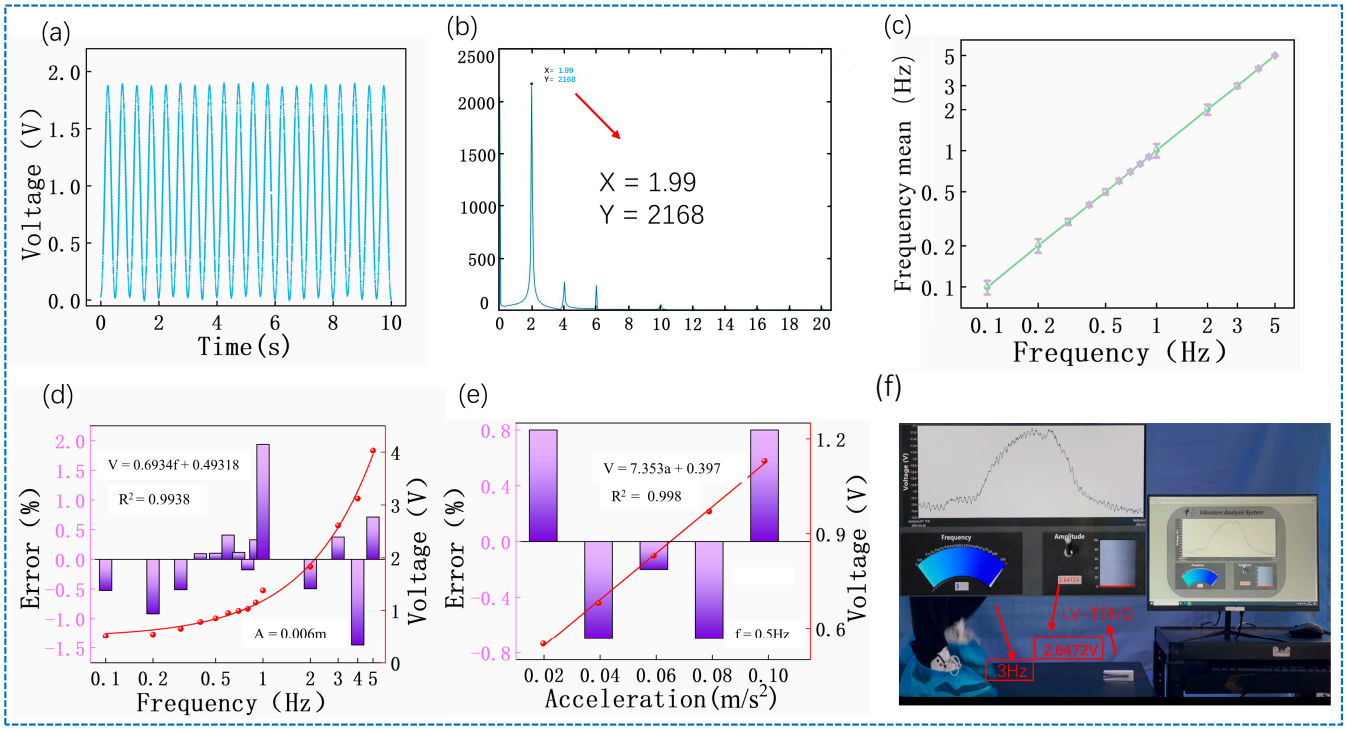

Figure 4. Performance of the LV-TENG as a low frequency vibration sensor. (**a**) Output voltage of the LV-TENG at f = 2.0 Hz and A = 6.0 mm; (**b**) FFT analysis on output signal at f = 2.0 Hz and A = 6.0 mm; (**c**) FFT analysis for frequency detection; (**d**) Linear fitting between vibration frequency and peak output voltage; (**e**) Linear fitting between vibration acceleration and peak output voltage; (**f**) Demonstration of the LV-TENG for low-frequency vibration monitoring.

In addition, the electrical output of the LV-TENG is positively related to the vibration parameters. Figure 4d,e show the variation of peak output voltage with the vibration in frequency and vibration acceleration under certain condition. Strong positive linear relationships are found between the output voltage with both the vibration frequency and acceleration, and the correlation coefficients after linear fitting are 0.994 and 0.998, respectively. Figures S2 and S3 in the supplementary indicate that the peak output current also has strong linear correlations with the vibration frequency and vibration acceleration, and the fitted linear coefficients are 0.986 and 0.995, respectively. Furthermore, it can be seen from the figure that the maximum measurement error under the studied vibration conditions is no more than 3%, which indicates that the LV-TENG as a vibration sensor is sensitive to low-frequency vibrations and has very high accuracy. The superior low-frequency vibration response characteristics of the LV-TENG indicate that its output can be used for the SHM analysis of marine engineering and even can be combined with structural seismology to trace the disturbance that caused the vibration.

Figure 4f demonstrates the application of the LV-TENG in low-frequency vibration sensing. The movement of humans can cause vibrations in the structure. A local enlargement showing the output information of the LV-TENG is displayed in Figure S5 of the supplementary. As can be seen from the figure and the demonstration Video S1 in the supplementary materials, the LV-TENG can detect low-frequency vibrations of the structure in real time.

4. Conclusions

Low-frequency vibration monitoring is an important part of SHM in the field of marine engineering. In this work, a low-frequency vibration sensor LV-TENG based on a cantilever-beam-structured triboelectric nanogenerator was proposed. It was designed to perform low-frequency vibration monitoring with high precision while realizing micro-energy capture. The LV-TENG was composed of a PLA frame with vibration-curve-structured design, two aluminum electrode layers, and a spring steel sheet covered with PTFE membranes. The main structure parameters, including the physical shape of the Al electrodes, the thickness of the cantilever beam, and the material of the dielectric layer, were optimized to enhance the electrical output of the LV-TENG. Results showed that the as-proposed LV-TENG can effectively harvest vibration energy and conduct vibration sensing within vibration frequency from 0.1 Hz to 5.0 Hz and amplitude from 2.0 mm to 10.0 mm. FFT analysis indicated that the LV-TENG can detect vibration frequency with an error less than 2%. In addition, the peak output voltage and current of the LV-TENG followed positive linear relationships with vibration parameters, and the fitted correlation coefficients were greater than 0.984. The demonstration experiment showed that the LV-TENG has provided a new idea for low-frequency vibration monitoring. The superior vibration response characteristics indicate that the output of the LV-TENG can be used for SHM analysis in marine engineering and even trace the disturbance that caused the vibration based on signal postanalysis.

Supplementary Materials: The following supporting information can be downloaded at: https://www.mdpi.com/article/10.3390/jmse11040838/s1, Figure S1: The specific structures of the three LV-TENGs with different Al electrodes; Figure S2: Linear fitting between vibration frequency and peak output current; Figure S3: Linear fitting between vibration acceleration and peak output current; Figure S4: Dependence of the output current and output power on the external load resistance; Figure S5: A local enlargement showing the output signal of the LV-TENG. Video S1: Demonstration of the LV-TENG for low frequency vibration monitoring induced by human movement.

Author Contributions: Conceptualization, X.X., M.X. and Q.W.; methodology, X.X., Q.W. and B.Y.; software, Q.W. and L.G.; validation, C.Z. (Cong Zhao) and B.Y.; formal analysis, C.Z. (Chuangqing Zhu) and L.G.; investigation, C.Z. (Cong Zhao) and L.L.; resources, M.X. and L.L.; data curation, C.Z. (Chuangqing Zhu) and L.G.; writing—original draft preparation, Q.W. and B.Y.; writing—review and editing, X.X.; supervision, X.X. and M.X.; project administration, M.X.; funding acquisition, X.X. All authors have read and agreed to the published version of the manuscript.

Funding: This research was funded by the National Natural Science Foundation of China (Grant No. 51906029) and the China Postdoctoral Science Foundation (2019M661084).

Institutional Review Board Statement: Not applicable.

Informed Consent Statement: Not applicable.

Data Availability Statement: Data is availability on request from the authors.

Conflicts of Interest: The authors declare no conflict of interest.

References

1. Kandasamy, R.; Cui, F.; Townsend, N.; Foo, C.C.; Guo, J.; Shenoi, A.; Xiong, Y. A review of vibration control methods for marine offshore structures. *Ocean Eng.* **2016**, *127*, 279–297. [CrossRef]
2. Liu, Y.; Meng, H.; Lv, W. Experimental Research on Vibration Transmission and Isolation for Ship's Seawater Piping System. In Proceedings of the International Conference on Advanced Mechanical Engineering (AME 2012), Wuhan, China, 7–8 July 2012; pp. 68–72.
3. Davydov, V.S. Recognition of Incipient Defects in the Units of Ship Machinery by Vibrodiagnostics Based on Optimum Decision Rules. *Russ. J. Nondestruct. Test.* **2019**, *55*, 185–191. [CrossRef]
4. Hu, D.; Guo, Y.; Chen, X.; Zhang, C. Cable Force Health Monitoring of Tongwamen Bridge Based on Fiber Bragg Grating. *Appl. Sci.* **2017**, *7*, 384. [CrossRef]
5. Huang, Y.; Dai, G. Study of Vibration Characteristics of The Reciprocating Compressor on The Offshore Platform Based on Harmonic Wavelet Packet Transform. In Proceedings of the International Conference on Advanced Material and Manufacturing Science (ICAMMS 2012), Beijing, China, 20–21 December 2012; pp. 2107–2112.
6. Wu, C.; Huang, H.; Li, R.; Fan, C. Research on the Potential of Spherical Triboelectric Nanogenerator for Collecting Vibration Energy and Measuring Vibration. *Sensors* **2020**, *20*, 1063. [CrossRef] [PubMed]
7. Tan, D.; Zhou, J.; Wang, K.; Zhao, X.; Wang, Q.; Xu, D. Bow-type bistable triboelectric nanogenerator for harvesting energy from low-frequency vibration. *Nano Energy* **2022**, *92*, 106746. [CrossRef]
8. Salauddin, M.; Toyabur, R.M.; Maharjan, P.; Rasel, M.S.; Kim, J.W.; Cho, H.; Park, J.Y. Miniaturized springless hybrid nanogenerator for powering portable and wearable electronic devices from human-body-induced vibration. *Nano Energy* **2018**, *51*, 61–72. [CrossRef]
9. Huang, J.; Bao, C.; Luo, A.; Wang, F. Mechanical Energy Harvester for Smart Shared Bicycle Application. In Proceedings of the 16th IEEE International Conference on Nano/Micro Engineered and Molecular Systems (IEEE-NEMS), Xiamen, China, 25–29 April 2021; IEEE: Toulouse, France, 2021; pp. 184–188.
10. Liu, J.; Liu, C.; Zhao, C.; Li, H.; Qu, G.; Mao, Z.; Zhou, Z. Design of Self-powered Environment Monitoring Sensor Based on TEG and TENG. In Proceedings of the 16th IEEE International Conference on Nano/Micro Engineered and Molecular Systems (IEEE-NEMS), Xiamen, China, 25–29 April 2021; IEEE: Toulouse, France, 2021; pp. 749–753.
11. Rodriguez, F.; Sanchez-Guardamino, I.; Martin, F.; Fontan, L. Non-intrusive, self-supplying and wireless sensor for monitoring grounding cable in smart grids. *Sens. Actuators A-Phys.* **2020**, *316*, 112417. [CrossRef]
12. Luo, J.; Wang, Z.L. Recent progress of triboelectric nanogenerators: From fundamental theory to practical applications. *Ecomat* **2020**, *2*, e12059. [CrossRef]
13. Niu, S.; Wang, Z.L. Theoretical systems of triboelectric nanogenerators. *Nano Energy* **2015**, *14*, 161–192. [CrossRef]
14. Pei, C.; Wu, C.-Y.; England, D.; Byard, S.; Berchtold, H.; Adams, M. Numerical analysis of contact electrification using DEM-CFD. *Powder Technol.* **2013**, *248*, 34–43. [CrossRef]
15. Wang, Z.L.; Chen, J.; Lin, L. Progress in triboelectric nanogenerators as a new energy technology and self-powered sensors. *Energy Environ. Sci.* **2015**, *8*, 2250–2282. [CrossRef]
16. Li, C.; Yin, Y.; Wang, B.; Zhou, T.; Wang, J.; Luo, J.; Tang, W.; Cao, R.; Yuan, Z.; Li, N.; et al. Self-Powered Electrospinning System Driven by a Triboelectric Nanogenerator. *ACS Nano* **2017**, *11*, 10439–10445. [CrossRef] [PubMed]
17. Yang, J.; Chen, J.; Su, Y.; Jing, Q.; Li, Z.; Yi, F.; Wen, X.; Wang, Z.; Wang, Z.L. Eardrum-Inspired Active Sensors for Self-Powered Cardiovascular System Characterization and Throat-Attached Anti-Interference Voice Recognition. *Adv. Mater.* **2015**, *27*, 1316–1326. [CrossRef] [PubMed]
18. Chen, J.; Zhu, G.; Yang, J.; Jing, Q.; Bai, P.; Yang, W.; Qi, X.; Su, Y.; Wang, Z.L. Personalized Keystroke Dynamics for Self-Powered Human-Machine Interfacing. *ACS Nano* **2015**, *9*, 105–116. [CrossRef] [PubMed]
19. Song, Y.; Wang, N.; Hu, C.; Wang, Z.L.; Yang, Y. Soft triboelectric nanogenerators for mechanical energy scavenging and self-powered sensors. *Nano Energy* **2021**, *84*, 105919. [CrossRef]
20. Qin, Z.; Yin, Y.; Zhang, W.; Li, C.; Pan, K. Wearable and Stretchable Triboelectric Nanogenerator Based on Crumpled Nanofibrous Membranes. *ACS Appl. Mater. Interfaces* **2019**, *11*, 12452–12459. [CrossRef]
21. Chen, H.; Lu, Q.; Cao, X.; Wang, N.; Wang, Z. Natural polymers based triboelectric nanogenerator for harvesting biomechanical energy and monitoring human motion. *Nano Res.* **2022**, *15*, 2505–2511. [CrossRef]
22. Niu, S.; Zhou, Y.S.; Wang, S.; Liu, Y.; Lin, L.; Bando, Y.; Wang, Z.L. Simulation method for optimizing the performance of an integrated triboelectric nanogenerator energy harvesting system. *Nano Energy* **2014**, *8*, 150–156. [CrossRef]
23. Huang, B.; Wang, P.; Wang, L.; Yang, S.; Wu, D. Recent advances in ocean wave energy harvesting by triboelectric nanogenerator: An overview. *Nanotechnol. Rev.* **2020**, *9*, 716–735. [CrossRef]
24. Lee, B.-Y.; Kim, D.H.; Park, J.; Park, K.-I.; Lee, K.J.; Jeong, C.K. Modulation of surface physics and chemistry in triboelectric energy harvesting technologies. *Sci. Technol. Adv. Mater.* **2019**, *20*, 758–773. [CrossRef]
25. Wang, S.; Niu, S.; Yang, J.; Lin, L.; Wang, Z.L. Quantitative Measurements of Vibration Amplitude Using a Contact-Mode Freestanding Triboelectric Nanogenerator. *ACS Nano* **2014**, *8*, 12004–12013. [CrossRef]
26. Salauddin, M.; Rana, S.M.S.; Sharifuzzaman, M.; Song, H.S.; Reza, M.S.; Jeong, S.H.; Park, J.Y. Highly Electronegative V2CTx/Silicone Nanocomposite-Based Serpentine Triboelectric Nanogenerator for Wearable Self-Powered Sensors and Sign Language Interpretation. *Adv. Energy Mater.* **2023**, *13*, 2203812. [CrossRef]

27. Seol, M.L.; Han, J.W.; Moon, D.I.; Yoon, K.J.; Hwang, C.S.; Meyyappan, M. All-printed triboelectric nanogenerator. *Nano Energy* **2018**, *44*, 82–88. [CrossRef]
28. Du, T.; Zuo, X.; Dong, F.; Li, S.; Mtui, A.E.; Zou, Y.; Zhang, P.; Zhao, J.; Zhang, Y.; Sun, P.; et al. A Self-Powered and Highly Accurate Vibration Sensor Based on Bouncing-Ball Triboelectric Nanogenerator for Intelligent Ship Machinery Monitoring. *Micromachines* **2021**, *12*, 218. [CrossRef] [PubMed]
29. Zhang, H.; Yang, Y.; Su, Y.; Chen, J.; Adams, K.; Lee, S.; Hu, C.; Wang, Z.L. Triboelectric Nanogenerator for Harvesting Vibration Energy in Full Space and as Self-Powered Acceleration Sensor. *Adv. Funct. Mater.* **2014**, *24*, 1401–1407. [CrossRef]
30. Wang, Z.; Zhang, F.; Li, N.; Yao, T.; Lv, D.; Cao, G. Self-Powered Multifunctional Triboelectric Sensor Based on PTFE/PU for Linear, Rotary, and Vibration Motion Sensing. *Adv. Mater. Technol.* **2020**, *5*, 2000159. [CrossRef]
31. Xiao, X.; Zhang, X.; Wang, S.; Ouyang, H.; Chen, P.; Song, L.; Yuan, H.; Ji, Y.; Wang, P.; Li, Z.; et al. Honeycomb Structure Inspired Triboelectric Nanogenerator for Highly Effective Vibration Energy Harvesting and Self-Powered Engine Condition Monitoring. *Adv. Energy Mater.* **2019**, *9*, 1902460. [CrossRef]
32. Rasel, M.S.; Maharjan, P.; Salauddin, M.; Rahman, M.T.; Cho, H.O.; Kim, J.W.; Park, J.Y. An impedance tunable and highly efficient triboelectric nanogenerator for large-scale, ultra-sensitive pressure sensing applications. *Nano Energy* **2018**, *49*, 603–613. [CrossRef]
33. Wang, Z.L. Triboelectric Nanogenerators as New Energy Technology for Self-Powered Systems and as Active Mechanical and Chemical Sensors. *ACS Nano* **2013**, *7*, 9533–9557. [CrossRef] [PubMed]
34. Ren, Z.; Wu, L.; Zhang, J.; Wang, Y.; Wang, Y.; Li, Q.; Wang, F.; Liang, X.; Yang, R. Trapezoidal Cantilever-Structure Triboelectric Nanogenerator Integrated with a Power Management Module for Low-Frequency Vibration Energy Harvesting. *ACS Appl. Mater. Interfaces* **2022**, *14*, 5497–5505. [CrossRef] [PubMed]